

Albumin Hydrogels Formed by Electrostatically Triggered Self-Assembly and Their Drug Delivery Capability

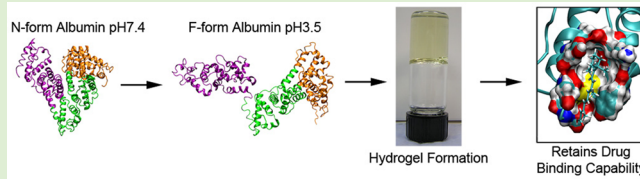
Kevin Baler,^{†,‡} Raman Michael,[†] Igal Szleifer,^{†,‡,§} and Guillermo A. Ameer*,^{†,‡,||}

[†]Department of Biomedical Engineering, [‡]Chemistry of Life Processes Institute, and [§]Department of Chemistry, Northwestern University, Evanston, Illinois 60208, United States

^{||}Institute for BioNanotechnology in Medicine, Northwestern University, Chicago, Illinois 60611, United States

Supporting Information

ABSTRACT: Biological hydrogels are fundamentally biocompatible and have intrinsic similarities to extracellular matrices in medical applications and drug delivery systems. Herein we demonstrate the ability to form drug-eluting protein hydrogels using a novel mechanism that involves the electrostatically triggered partial denaturation and self-assembly of the protein via changes in pH. Partial denaturation increases the protein's solvent exposed hydrophobic surface area, which then drives self-assembly of the protein into a hydrogel within 10 min at 37 °C. We describe the properties of an albumin hydrogel formed by this mechanism. Intrinsic drug binding properties of albumin to all-trans retinoic acid (atRA) are conserved through the partial denaturation process, as confirmed by fluorescence quenching. atRA released from the hydrogel inhibited smooth muscle cell migration as per an *in vitro* scratch wound assay. Atomistic molecular dynamics and potential of mean force calculations show the preservation and potential creation of new atRA binding sites with a binding energy of -41 kJ/mol . The resulting hydrogel is also biocompatible and exhibits rapid postgelation degradation after its implantation *in vivo*. This interdisciplinary work provides a new tool for the development of biocompatible protein hydrogel drug delivery systems.



INTRODUCTION

Serum albumin is widely used clinically as a critical component in solubilizing diagnostic and therapeutic products due to its versatility as a drug carrier.¹ Concurrently, biological hydrogels are extensively used in medical applications due to their fundamental biocompatibility and intrinsic similarities to the extracellular matrix of certain tissues.^{2,3} Hydrogels have been synthesized from a variety of biomacromolecules, such as serum albumin, by forming intermolecular cross-links via thermal or chemical methods.^{2,3} However, these approaches to albumin hydrogels do not account for the structural-functional changes that occur in the protein as a result of complexation or thermal denaturation. Proteins are complex biomacromolecules with well-established hierarchical structure from the primary sequence of amino acid residues to multiprotein assemblies at the quaternary level. The structural complexity of a single protein's three-dimensional structure (tertiary level) depends on the delicate interplay between electrostatic, hydrophobic, hydrogen bonding, and other interactions whose modification can result in significant conformational changes.⁴ Evolutionary optimization of these interactions in physiological environments has resulted in protein conformations that are functionally operational. Computational modeling studies of albumin show that electrostatic charges on the protein can be modified by changes in the solution pH to partially denature the original protein structure and expose hydrophobic regions.⁵ We hypothesize that these newly exposed regions can drive new quaternary assemblies leading to biological hydrogel formation

while preserving functional binding domains. Development of biomaterials that employ this generalizable mechanism could result in novel and unexpected hydrogel systems comprised entirely of biomacromolecular building blocks for use as drug delivery depots.

Serum albumin is a 66 kDa water-soluble protein and the most abundant protein in blood plasma (40–50 mg/mL). It serves as the primary carrier of various solutes in plasma, including cations, bilirubin, fatty acids, and therapeutic drugs.¹ There is extensive literature regarding serum albumin's affinities to various compounds,⁶ denaturation conditions,^{4,7–9} gelation mechanisms,^{10–15} and current or potential medical uses.^{16–21} Although albumin hydrogels have been formed by thermal denaturation, chemical cross-linking (e.g., glutaraldehyde), or polymer–albumin conjugates,^{1,20,22,23} these conditions are not found in the physiological environment. These hydrogel systems typically require either extensive protein denaturation (thermal) or chemical modification of the albumin, which can hamper protein functionality and compromise biocompatibility.

Electrostatically triggered albumin self-assembly takes advantage of the fact that albumin has the ability to reversibly and drastically change its conformation when exposed to changes in solution pH (transitions occurring at pH 2.7, 4.3, 8, and 10).^{1,4} For example, at pH 7.4, albumin has a normal heart-

Received: June 16, 2014

Revised: August 3, 2014

Published: August 22, 2014



like structure (N-form), while at pH 3.5, it has an expanded cigar-like structure (F-form).^{4,24} During the N–F form transition, bovine serum albumin (BSA) passes through the isoelectric point at pH 4.7, and the net charge on the protein changes from -16 at pH 7.4 to +100 at pH 3.5. Low solution pH also shifts the denaturation temperature of BSA from 62 °C at pH 7.4 to 46.8 °C at pH 3.5.²⁵ Our previous work has determined the structure of albumin through atomistic molecular dynamics simulations at pH 3.5 and suggested hydrophobic interactions and counterion binding as key drivers for protein aggregation in this system.⁵ Herein we report results that exploit this phenomenon and provide an example of how albumin hydrogels can be used for controlled drug delivery.

MATERIALS AND METHODS

Materials and Hydrogel Synthesis. BSA gel precursor solutions were formed by adding deionized water to essentially fatty acid free bovine serum albumin (A6003, Sigma, St. Louis, MO) in concentrations ranging from 9 to 20 wt % (1.4–3 mM). Solutions were stirred at 200–300 rpm until complete dissolution (~2–3 h). To form pH-induced bovine serum albumin gels (PBSA), the pH of the precursor solution was lowered to pH 3.5 by dropwise addition of 2 M HCl with constant stirring followed by submersion in a water bath at 37 °C for 2 h. To form thermally denatured bovine serum albumin gels (TBSA), the precursor solution was neutralized to pH 7.4 by 2 M NaOH followed by submersion in a water bath at 80 °C for 2 h. Precursor solutions were sterilized with a 0.2 μm nylon syringe filter before gelation (Fisher Scientific, PA). After formation, all samples were equilibrated in solution to leach out acid components equally. During this leaching procedure, there is no change in the swelling of the hydrogel samples.

Atomistic BSA Model Simulations. The structure of partially denatured BSA was obtained from previous work.⁵ Briefly, molecular dynamics simulations were performed on BSA whose protonation state was set to pH 3.5, as determined by FAMBE-pH, a program that calculates the total solvation free energies of proteins as a function of pH.²⁶ After randomly adding 10 molecules of atRA to the system, molecular dynamics simulations were performed using the GROMACS simulation package at constant temperature (300 K) and pressure (1 atm).^{27–30} The OPLS/AA force field was used to simulate the atomistic BSA model (9336 atoms) solvated with ~94000 SPC water molecules, 100 counterions, and 10 atRA molecules.^{30,31} The atRA-BSA models were equilibrated by a steepest descent algorithm followed by a 100 ns NVT production run with periodic boundary conditions.

Potential of Mean Force Calculation. The potential of mean force was calculated from a series of umbrella sampling³² simulations ($n = 30$), where configurations of bound atRA molecules were placed at linearly increasing distances ($\Delta z = 0.5 \text{ Å}$) from their self-selected preferred binding pocket after 100 ns of unconstrained molecular dynamics. The center of mass of the atRA molecule and the center of mass of neighboring binding pocket residues were used as the anchor points to determine the separation distance z between the BSA binding site and atRA. The potential of mean force was then calculated on the output of the 30 simulations after five ns using the weighted histogram analysis method (g_wham) embedded in the GROMACS software.³³ The number of configurations and separation distances were selected such that the entire phase space was sufficiently sampled until z is at least two nm from the binding site, where $z = 0$ is the preferred binding distance after 100 ns.

Cryo-SEM Imaging. PBSA and TBSA gels were vitrified with a controlled environment vitrification system (CEVS, custom built courtesy of the Talmon Group, Technion, IL).^{34,35} Briefly, the CEVS consists of four modules: (1) temperature control module, (2) environmental chamber, (3) plunge module, and (4) cryogen box. CEVS is operated in a fume hood to pump away nitrogen gas and possibly small amounts of ethane vapor while maintaining the room air-conditioned at 20 °C to reduce ambient humidity. Samples (3 μL)

are loaded onto planchettes, and a copper grid is immersed in the sample. A second planchette is placed over the sample facedown, making a spring-loaded planchette sandwich and is then locked into a plunging tweezer module. A cable release mechanism simultaneously opens a trap door in the CEVS and plunges the tweezers with the planchette sandwich into the cryogen box that contains liquid ethane in an LN₂ bath. The planchette sandwich is then moved from the liquid ethane into the LN₂ bath and transferred to a BAL-TEC BAF060 for further processing (BAL-TEC, Austria). The spring-loaded planchette sandwich is opened, which fractures the sample surface, and then freeze etched by raising the temperature to sublimate water from the surface. A thin Pt/C coating several nm thick is coated onto the fracture surface and then transferred to a Zeiss Ultra plus HR-SEM for cryo-SEM imaging (Zeiss, Thornwood, NY).

Mechanical Indentation of BSA Gels. A custom built micro-indententer (Shull Group, Northwestern University, IL) was used to measure the Young's modulus of BSA gels.³⁶ A flat-ended cylindrical stainless steel punch with a radius $a = 0.44 \text{ mm}$ was used to indent the surface of the gel with a Burleigh inchworm motor (Rochester, NY) attached to a Sensotec 1 kg load cell (Columbus, OH), while the displacement was measured with a Philtec optical displacement sensor (Annapolis, MD). As the probe indented the sample at a fixed rate (10 μm/s), the load was recorded on a computer. The following eq 1 is the relationship between the load P and displacement δ in the linear regime of the curve:

$$\frac{P}{\delta} = \frac{8aE}{3f_c(a/h)} \quad (1)$$

This relationship can be used to convert the recorded loads into stresses for determination of the Young's modulus. The term, f_c , is a geometric confinement factor determined by the ratio of the indenter radius to the gel thickness h which, in this work, is ~1. Rewriting eq 1 yields an expression for the average stress σ_{avg} under the indenter:

$$\sigma_{\text{avg}} = \frac{P}{\pi a^2} = \frac{8E}{3\pi} \left(\frac{\delta}{a} \right) \frac{1}{f_c(a/h)} \quad (2)$$

The slope of the curve in the linear regime can be used to calculate the Young's modulus E during the indentation. For low values of a/h , where $f_c = 1$, the quantity δ/a functions as the effective strain. All differences (between conditions and concentrations) are significant at $p < 0.001$ levels.

Rheological Characterization of BSA Gels. PBSA (pH 3.5) and TBSA precursor solutions were made at several concentrations (20, 18, 16, 14, 12 wt %). The amount of water added to each polymer solution was calculated to give the final polymer concentration. Rheometric characterization was performed on Discovery Hybrid Rheometer (TA Instruments, New Castle, DE) equipped with a Peltier hood and evaporation blocker. Samples were heated to either 37 (PBSA) or 80 °C (TBSA) to evaluate the gelation kinetics for both gel types. Small 0.5% oscillatory strain was applied throughout the experiment while measuring the sample storage and loss modulus over time. The onset of hydrogel formation is defined as the crossover between the storage and the loss modulus.

In Vivo Subcutaneous Rat Model. Eight female Sprague-Dawley rats (Harlan Laboratories, Inc.) weighing 150–175 g were used for in vivo biocompatibility testing of the BSA gels. Four rats were randomly assigned into two groups for explant time points at 4 days and 4 weeks for evaluation of the acute and chronic inflammatory response. Animals were anesthetized using the inhalant machine Impact 6 (Vetequip Inc., Pleasanton, CA). Isoflurane was administered at a concentration of 2% with an oxygen flow rate of 2 L/min. Following anesthesia, the backs of the animals were shaved and then disinfected with butadiene followed by alcohol and a second butadiene wipe. Two incisions of approximately 1.5 cm in length were made at the implantation sites and subcutaneous pockets were created by blunt dissection in each location. The 20 wt % albumin hydrogels (both PBSA and TBSA) were fabricated as described in Materials and Methods and were cut into disks ($h = 0.5 \text{ cm}$, $r = 0.6 \text{ cm}$) using a sterile biopsy punch. In one location, an acid leached 20 wt % PBSA

gel disk was implanted into the subcutaneous pocket far from the incision site. At the other incision site, a 20 wt % TBSA gel disk was implanted. A control saline injection and pH 7.4 (20 wt %) BSA solution was injected into the back of the rat in the two remaining implantation sites. Each disk or injection had a volume of 0.5 mL. In all, each rat received all four treatments (PBSA, TBSA, BSA solution, saline) in four different rotating locations (anterior right, anterior left, posterior right, posterior left) for both time points (four day and four week). The wounds were closed with surgical staples and implants were subsequently removed after 4 days. At each time point, four animals were anesthetized and subsequently euthanized via CO₂ asphyxiation. Cervical dislocation was performed as a secondary euthanasia method and the explants were harvested. The explants, which included the tissues surrounding the implanted material, were snap frozen in a dry ice/acetone mixture. Explants were stored at -80 °C until sectioning and H&E staining. Stained sections were photographed in series and in adjacent regions along the dorsoventral axis from the interior of the implant to the skin surface. The Northwestern University Animal Care and Use Committee approved all animal procedures used in this work.

atRA Binding and Release. All-trans retinoic acid (atRA, R2625, Sigma, St. Louis, MO) was added to solutions of BSA with molar ratio concentrations including 0:1, 0.08:1, 0.1:1, 0.13:1, 0.2:1, 0.4:1, 0.8:1, 1.2:1, 1.6:1, and 2:1 (atRA/BSA). A baseline fluorescence intensity of BSA at pH 7.4 and 3.5 measured at 340 nm with excitation at 295 nm was recorded ($n = 4$ for each molar ratio concentration), as reported in the literature³⁷ using the plate reader Tecan Safire II (Tecan, Maennedorf, Switzerland). Then, atRA binding to BSA at pH 7.4 and 3.5 was assessed immediately after the addition of atRA at the different molar ratios. For measuring atRA release from hydrogel disks, a higher molar ratio concentration of 8:1 (atRA:BSA) was used when incorporating atRA into BSA precursor solutions before gelation. Precursor solutions were processed as normal to fabricate atRA-loaded PBSA and TBSA hydrogel disks with a final volume of 0.5 mL. Disks were submerged in 10 mL of PBS at 37 °C for atRA release studies. Eluates were collected and replaced at 1, 3, 6, 12, 24, 48, 72, 144, and 240 h sampling times and a fluorescence intensity of atRA at 340 nm and BSA at 280 nm was collected with a NanoDrop 2000C Spectrophotometer (ThermoScientific, Waltham, MA).

Scratch Test Migration Assay. Human aortic smooth muscle cells (HASMC; Lonza, Basel, Switzerland; passage five) were cultured in SmGM-2 media. All cells were cultured at 37 °C in a humidified incubator containing 5% CO₂. HASMCs (seeding density 1×10^4 cells/cm²) were seeded onto TCP surfaces and grown until 90% confluent. Cell culture media was changed every 2 days until confluence, after which serum-free SmGM-2 media was used to create a nutrient-starved environment for 24 h. A vertical scratch was made with a sterile 200 μ L pipet tip in the confluent HASMC layer, rinsed with warm PBS, and replaced with 1 mL of SmGM-2 media. The underside of the dish was marked near the wound area to aid in identification. Wells were randomly placed into four groups that received either a 100 μ L dose of eluted material from atRA loaded PBSA or TBSA release study at day 10, a 100 μ L dose of 24 ng atRA dissolved in PBS, or a control of 100 μ L of PBS. A light microscope (Nikon Eclipse TE2000-U) was used to capture images using Image Pro 5.0 software (MediaCybernetics, Bethesda, MD) of the wound area immediately at day 0 and at various times until the control wound closed at 24 h. Wound areas were determined using an automated wound area measurement macro with the ImageJ 1.43r software (NIH, Bethesda, MD). The measurement of migration was determined by subtracting the cell-free area at day 0 from the cell-free area at 24 h. Data were presented as means \pm SD of several independent experiments from each atRA-loaded hydrogel replicate.

Data Analysis. Data analysis was performed using Microsoft Excel software. Data from independent experiments were quantified and analyzed for each variable. Comparisons between multiple treatments were made with a student's *t* test. A *p*-value of <0.05 was considered to be statistically significant.

RESULTS

Fabrication of Albumin Hydrogels by Electrostatically Triggered Self-Assembly. Albumin dissolved in deionized water formed a clear yellow solution. During dropwise addition of 2 M HCl, transient changes in turbidity were observed visually as the N-form albumin partially denatured to the F-form albumin, represented by the model of albumin undergoing this transition (Figure 1A). In concentrated solutions >15 wt %

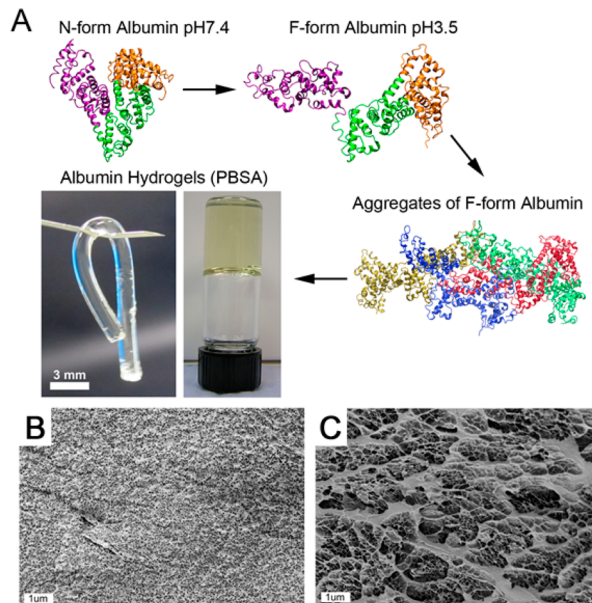


Figure 1. Formation of albumin hydrogels by electrostatically triggered partial protein denaturation. (A) Ribbon diagrams depicting the partial denaturation of N-form to F-form albumin leading to protein–protein aggregation and eventual hydrogel formation. Inverted vial depicts 20 wt % PBSA formed at 25 °C. Tubular PBSA cylinder made in mold at 37 °C. Cryo-SEM images of freeze-fractured hydrogels formed by electrostatic triggering method at pH 3.5 at 37 °C (B) or by thermal denaturation at 80 °C method (C).

with an optimal final pH 3.5 (Figure 2), these partially denatured structures aggregate together and self-assemble into a solid hydrogel network within ~24 h at room temperature or in 10 min at 37 °C (Figure 1A). Accelerated 10 min hydrogel formation was achieved by placing small volumes of partially denatured albumin solutions (~100 μ L) inside tubular molds (3 mm diameter) in the 37 °C water bath with the effect of accelerated thermal equilibrium. Fabrication of larger volumes of albumin solutions >500 μ L were made in cell culture wells or scintillation vials and submerged in 37 °C for 2 h to ensure hydrogel formation. In contrast, BSA precursor solutions at pH 7.4 do not exhibit any gelation behavior unless the temperature rises above 62 °C to achieve thermal denaturation of the N-form. While PBSA and TBSA hydrogel appear identical at the macroscale, Cryo-SEM imaging reveals stark differences between the two hydrogels. Figure 1B shows PBSA hydrogels to have a compact structure with small pores, while Figure 1C shows TBSA hydrogels to have an expanded structure with larger pore sizes.

To characterize the ideal pH range where PBSA hydrogels can form, hydrogels were subjected to compressive mechanical indentation testing to measure their Young's moduli. The strongest PBSA hydrogels were formed in the F-form pH range between 3.0 and 4.0 (Figure 2A). Above pH 4, the transition

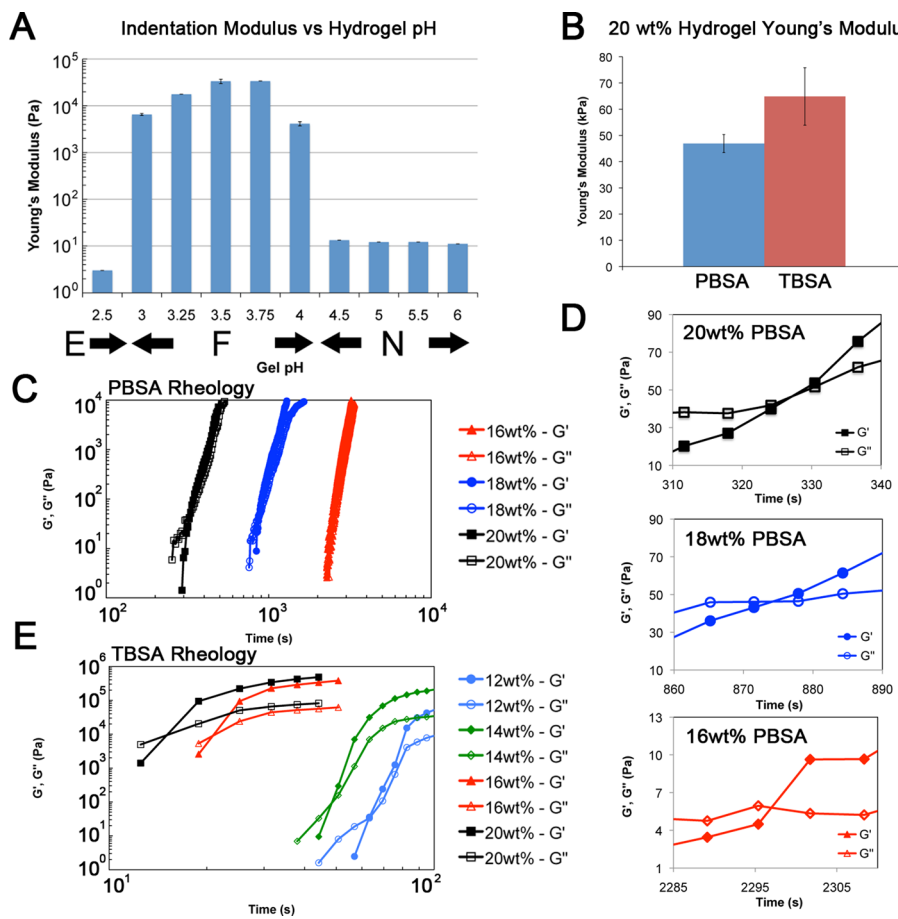


Figure 2. Mechanical properties of BSA hydrogels demonstrating PBSA hydrogels are softer than TBSA hydrogels. (A) Young's modulus of BSA solutions (17 wt % BSA) with different pH values ranging from 2.5 to 6 incubated at 37 °C ($n = 4$ for each pH value). BSA forms (E, F, N) are mapped below the plot according to their pH transition values. (B) Young's modulus of 20 wt % PBSA (pH 3.5 incubated at 37 °C, $n = 4$) and 20 wt % TBSA (pH 7.4 incubated at 80 °C, $n = 8$) hydrogels measured by mechanical indentation. Error bars in (A) and (B) represent the standard deviation of the data set. (C) Rheological characterization of PBSA formation kinetics for protein concentration 20, 18, and 16 wt %. (D) Crossover points between G' and G'' for each concentration of PBSA at 20, 18, and 16 wt %. (E) Rheological characterization of TBSA formation kinetics for protein concentration 20, 18, 16, 14, and 12 wt %.

from the N-form albumin to the F-form albumin was incomplete and these solutions did not form solid PBSA gels. Below pH 3.0, BSA gel solutions became highly viscous but never formed a solid gel. Maximal gel modulus (34 kPa) was achieved at pH 3.5 for 17 wt % PBSA hydrogels.

Comparison of the Young's modulus between PBSA and TBSA hydrogels with the same protein concentrations indicates that the TBSA hydrogels are stronger than the PBSA hydrogels (Figure 2B). The 20 wt % PBSA and TBSA hydrogels were used for the remainder of this work, with Young's modulus values of 46 and 67 kPa, respectively. Rheological characterization of PBSA and TBSA samples in different concentrations demonstrate the gelling kinetics for the two types (Figure 2C–E). PBSA hydrogels in several different concentrations (16, 18, 20 wt %) form after several minutes (2301.7s, 887.8s, 330.5s), as defined by the crossover between the G' and G'' curves (Figure 2C,D) after temperature reaches 37 °C. The PBSA hydrogels at the 12 and 14 wt % concentration never had a crossover after 2 h of testing (not shown). This finding delineates a critical minimum protein concentration of ~15 wt % albumin for PBSA hydrogel formation. In contrast, the TBSA hydrogels in several different concentrations (12, 14, 16, 18, 20 wt %) formed very quickly (69.5s, 50.7s, 25.2s, 18.8s, 17.9s), as defined by the crossover between the G' and G'' curves (Figure

2E) after the temperature reaches 80 °C. For clarity, the crossover curves representing 18 wt % are not shown.

PBSA Acid Neutralization and Effect of Chemical Environment on Hydrogel Integrity. To assess the nature of the interactions within the gel network, 20 wt % PBSA gel samples (pH 3.5) were incubated in different chemical environments (Figure 3). PBSA hydrogels formed at low pH were stable after acid neutralization to pH 7 by acid leaching in a PBS water bath. Phenol red added to neutralizing PBS buffer colored the PBSA hydrogels red over 3 days and serve as a visual marker for bulk hydrogel pH. PBSA hydrogels were stable for up to three months in deionized H₂O (pH 7.32), HCl–H₂O (pH 3.59), NaOH–H₂O (pH 10.28), and in PBS (pH 7.53), indicating a resistance to degradation by acidic or basic conditions. PBSA gels submerged in 8 M urea or 10% SDS were completely degraded within 17 h indicating that a primary mechanism of PBSA hydrogel formation is non-covalent and probably driven by hydrophobic interactions. Reduction of intermolecular disulfide bonds by β -mercaptoethanol (β -ME) solvent resulted in hydrogel swelling by a ~4× volume increase.

In Vivo Biocompatibility Evaluation. To evaluate the acute and chronic inflammatory potential of the BSA hydrogels in vivo, TBSA and acid-leached PBSA gel disks were implanted

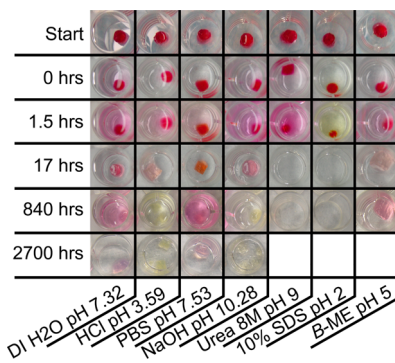


Figure 3. Effect of various chemical environments on PBSA hydrogel integrity. Small cylindrical PBSA hydrogels (0.5 cm diameter), acid-leached in DMEM for 3 days until the pH returned to neutral pH, were placed in different solutions and photographed over the course of three months. These images are representative of the larger sample set ($n = 4$) and demonstrate hydrogel degradation resistance to acid, base, and salt conditions. Urea and 10% SDS degrade the gels within 17 h while disulfide bond reduction by β -ME results in hydrogel swelling.

subcutaneously. Gross observation of the explants at 4 days and 4 weeks showed that the tissue had grown around the implants. H&E staining of the sections revealed stark differences between the degradation patterns of the PBSA and the TBSA implants *in vivo* (Figure 4). Cells infiltrating the PBSA hydrogels were seen at both time points, and correlated with significant gel degradation (Figure 4a,e). The PBSA hydrogels were noticeably more degraded at 4 weeks than at 4 days although both displayed complete degraded channels traversing the entire length of the implant. In contrast, TBSA hydrogels showed no

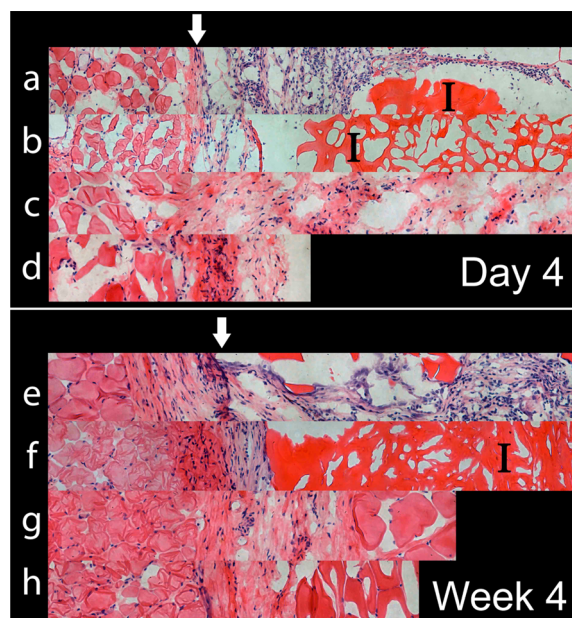


Figure 4. Biological response to subcutaneously implanted PBSA and TBSA hydrogels. Tissues with implanted PBSA gel disks (a, e), TBSA gel disks (b, f), pH 7.4 BSA solution injection (c, g), and saline control injections (d, h) at 4 days (a–d) and 4 weeks (e–h). Samples were stained with H&E: purple, nuclei; pink, cytoplasm; pink-red/I, implant gels. Histological images are aligned to each other at the original interface (white arrow) between the implant and the tissue lining the subcutaneous pocket. Images for each time point are from the same rat and are representative of the group population overall ($n = 4$).

sign of degradation and were intact at both time points (Figure 4b,f). A fibrous capsule surrounding the TBSA hydrogels became denser and thicker at 4 weeks relative to 4 days. Control 20 wt % BSA solutions (pH 7.4) injected into subcutaneous pockets resulted in an increased general inflammatory response judged by relative increase in number of cells in the subcutaneous pocket (Figure 4c) at 4 days when compared to the saline control injection (Figure 4d). At 4 weeks, the inflammatory response of the BSA injection has decreased significantly (Figure 4g) and was similar to that of the saline control (Figure 4h).

atRA Binds to Both F-Form Albumin and N-Form Albumin Isoforms. Tryptophan fluorescence at 340 nm changes upon atRA binding to BSA (Figure 5). One of the two tryptophans in BSA (TRP 213) is located deep within the globin fold in domain II and fluorescence signal from this tryptophan is reduced when bound to atRA (Figure 5A). Without added atRA, N-form albumin exhibits higher initial fluorescence intensity over F-form albumin (Figure 5B). Upon addition of atRA, the tryptophan fluorescence signal at 340 nm is rapidly quenched for both N-form albumin and F-form albumin. As a fraction of the initial fluorescence signal, N-form albumin exhibits greater fluorescence quenching than F-form albumin (Figure 5C) that may be due to the altered conformation state of F-form albumin and shifting atRA binding sites to other locations not dominated by the TRP 213 residue. PBSA and TBSA hydrogels loaded with atRA demonstrate a small initial burst release of atRA followed by linear release over 10 days in PBS at 37 °C (Figure 5D).

atRA Binding Sites Determined by Molecular Dynamics. Computational molecular dynamics enables atomic level resolution of the interaction between albumin and atRA during several binding events. Initial random placement of atRA molecules in albumin models for N-form albumin and F-form albumin structures allow for unbiased exploration and binding of atRA molecules to the protein surfaces. Final configurations of atRA on N-form albumin and F-form albumin conformations are represented in Figure 6. Videos showing the entire simulation are available in the Supporting Information (Videos S1 and S2). For both structures, there are sites on the protein that were bound to a single atRA molecule (FSite1, FSite2, FSite3, NSite1, NSite2, and NSite3) and areas where clusters of atRA molecules formed an aggregate (FSite4 Cluster, NSite4 Cluster). These clusters were not formed in the water phase but rather formed after an initial atRA molecule became bound to the cluster site. In N-form albumin, atRA molecules were bound to all three domains while F-form albumin had no atRA molecules bound to domain III (Figure 6, top purple). Domain III experiences the greatest degree of denaturation during the N–F transition. atRA binding events on both N-form albumin and F-form albumin were, within the time scale of the simulation, irreversible. When an atRA molecule would approach the surface of the protein near a binding site, it would remain localized to that site as quantified by the successive drop in the separation distance between each atRA molecule and its nearest protein residue surface (Figure 7A,B). Within 80 ns, 9 out of 10 atRA molecules were bound to the F-form albumin protein surface, while all 10 atRA molecules were bound to the N-form albumin surface.

Potential of Mean Force Calculation for atRA Binding to FSite1 and NSite1. The potential of mean force (PMF) is the free energy of interaction between two molecules. It represents the interaction between the molecules at a fixed

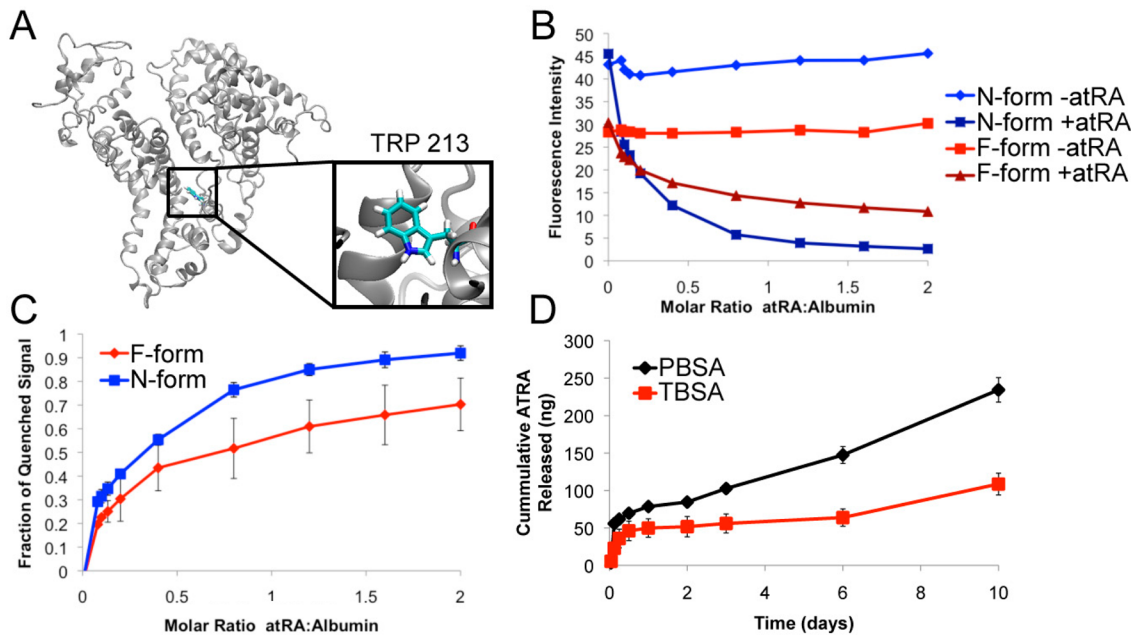


Figure 5. atRA binding to N-form albumin and F-form albumin measured via fluorescence quenching of tryptophan residue TRP 213 at 340 nm (A). Fluorescence intensity for N isoform BSA and F isoform BSA is consistent before addition of atRA (B). Addition of increasing molar concentration of atRA quenches both N-form albumin and F-form albumin fluorescence intensity. (C) A greater fraction of initial fluorescence is quenched in N-form albumin than in F-form albumin indicating altered binding affinity. (D) Release of atRA into PBS at 37 °C from F-form albumin and TBSA hydrogels.

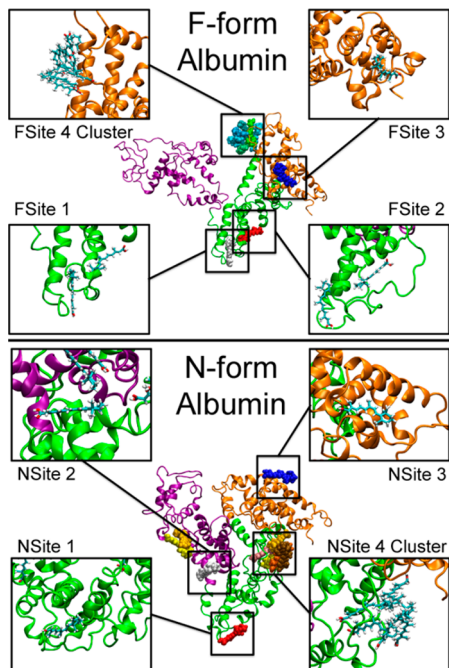


Figure 6. Localization of 10 atRA molecules binding to F-form albumin and N-form albumin after fully atomistic MD simulations for 100 ns. Top panel depicts F-form albumin binding sites located primarily in domains I (orange) and II (green). Clusters of atRA also formed aggregates on the protein surface. Bottom panel depicts N-form albumin binding sites located in all three domains.

separation averaged over all the degrees of freedom of the system, for example, water molecules, intermolecular and intramolecular interactions, and possible rotation and conformations of the protein and the atRA. Therefore, it provides the value for the work required to bring an atRA molecule from

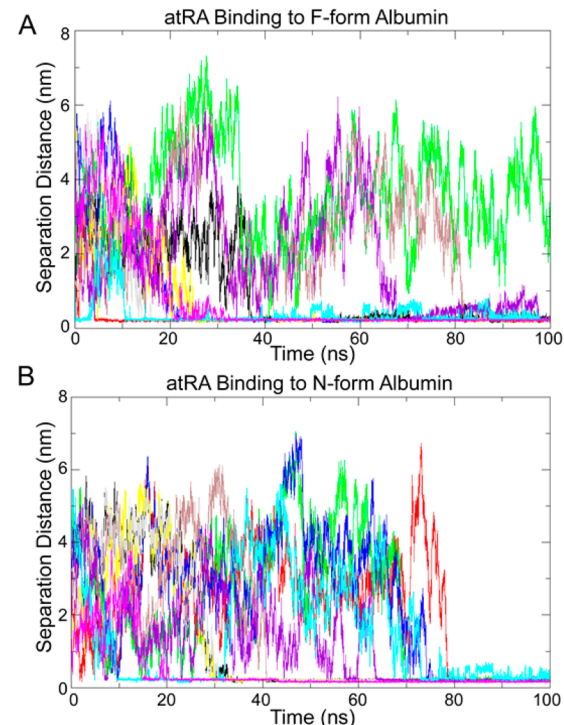


Figure 7. Separation distance between individual atRA molecules and their nearest protein surface residues during 100 ns MD simulations for both F-form albumin (A) and N-form albumin (B). Each individual atRA molecule is uniquely colored and becomes bound to the protein surface when the separation distance drops below 0.14 nm. atRA molecules that bind to the surface become effectively immobilized within 100 ns time scale of the simulation. At the end of the simulation, 9 out of 10 atRA molecules are bound to F-form albumin, while 10 out of 10 atRA molecules are bound to N-form albumin.

the bulk to a distance z from a BSA binding site. The potential of mean-force difference between infinity separation, defined as zero, and that of the minimum represents the free energy of binding. Our objective in calculating the PMF for FSite1 and NSite1 is to evaluate whether the F-form albumin conformations locked in the PBSA hydrogels retain atRA binding affinity comparable to N-form albumin. Literature estimates the binding energy for the fluorescence-quenching TRP 213 atRA binding site on N-form albumin are -31.7 kJ/mol .³⁷ Our PMF calculations show the FSite1 has a binding energy of -41 kJ/mol and the NSite1 has a binding energy of -13 kJ/mol (Figure 8). The optimal separation distance between the center

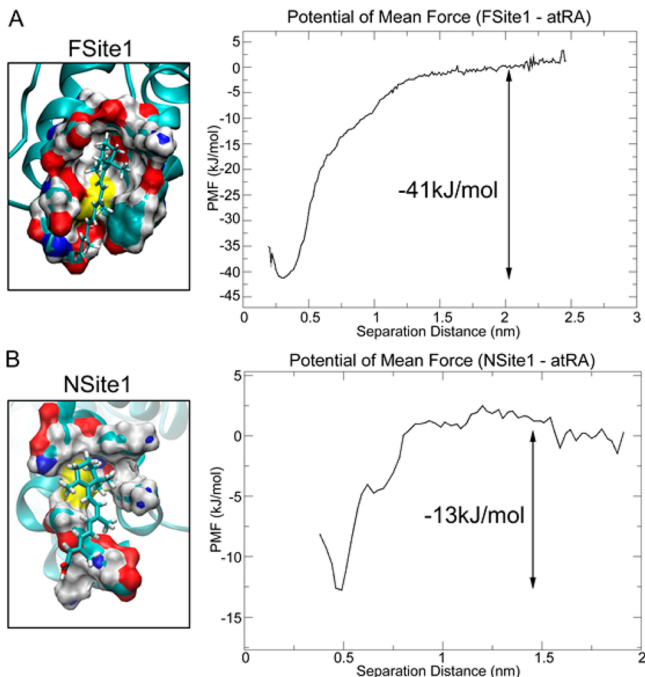


Figure 8. Potential of mean force calculations from umbrella sampling simulations for atRA molecules entering Site 1 on both F-form albumin and N-form albumin. In this particular site, the $\Delta G = -41 \text{ kJ/mol}$ for Site 1 on F-form albumin (A) and $\Delta G = -13 \text{ kJ/mol}$ for Site 1 on N-form albumin (B).

of mass of atRA and the center of mass on FSite1 is 0.32 nm and with NSite1 it is 0.48 nm. Taken altogether, these results demonstrate that the F-form albumin conformation retains a strong binding affinity toward atRA.

Released atRA Inhibits HASMC Migration. The bioactivity of atRA released from PBSA or TBSA gels was evaluated in a scratch wound assay. After allowing HASMCs to grow to 90% confluence and migration priming in serum-starved media, elution from day 10 window (containing 75 ng/mL atRA) of the release study was further diluted to 24 ng/mL with PBS and added to the cell culture. As expected, the migration of positive control cells exposed directly to 24 ng/mL atRA added in the media was inhibited in comparison to the negative control cells without atRA exposure (Figure 9). This result confirms the initial bioactivity of the atRA to inhibit HASMC migration. HASMC migration for cells receiving atRA released from PBSA and TBSA gels was also inhibited and significantly different from the negative control.

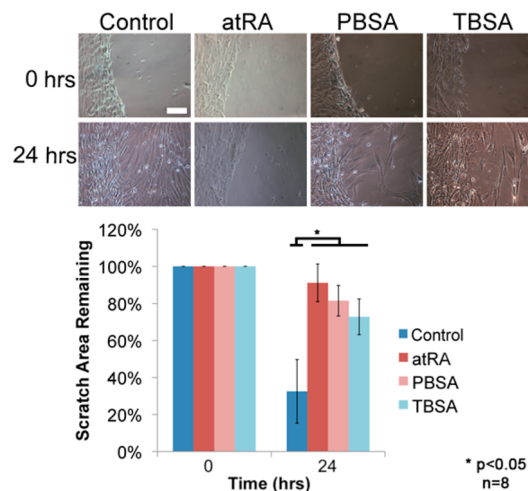


Figure 9. atRA released from PBSA and TBSA hydrogels remains bioactive and reduces the migration of smooth muscle cells as evaluated by a 24 h scratch wound assay. All cultures are serum starved to limit proliferation. Compared to controls, all cells exposed to atRA (direct atRA, eluted from PBSA, and eluted from TBSA) exhibited a significant ($p < 0.05$) reduction in cell migration. Scale bar = 100 μm .

DISCUSSION

Albumin has recently gained importance as a component of diagnostic and therapeutic products. Due to its versatility to bind a wide range of molecules and its biocompatibility, it is an attractive building block for novel drug-eluting hydrogels.¹ To maintain a high degree of biocompatibility and maximize binding site functionality it is desirable to not chemically modify the protein with cross-linkers to form the gels. In this work, we report on the fabrication of a new class of albumin hydrogels by the exploitation of intrinsic partial denaturation pathways that allows hydrogel formation without compromising binding site functionality. We report a critical threshold albumin concentration and a pH range that is conducive to the electrostatically triggered formation of hydrogels referred to as PBSA gels. This concentration was almost three times higher than the critical concentration required for the formation of TBSA gels.³⁸ The difference in critical protein concentrations and the kinetics of hydrogel formation required to form PBSA or TBSA gels suggests that these two protein denaturation pathways are substantially different. Others have shown that TBSA gelation is caused by a viscoelastic phase separation that locally increases the gel concentration that precedes the formation of percolating gel networks in these systems.¹⁰ Our experimental data, together with computational results, are consistent with electrostatically mediated partial denaturation of albumin that exposes hydrophobic protein domains and causes protein self-assembly. This pH-dependent albumin gelation was biphasic, preserved atRA binding domains, and possibly created new ones.

Mechanical indentation testing and rheological characterization was used to evaluate the mechanical and kinetic gel formation properties for PBSA and TBSA hydrogels.^{36,39} The elastic modulus of PBSA gels (46 kPa) were also different from those of TBSA gels (67 kPa), the latter being more stiff. Similar cross-linked 15 wt % TBSA type-hydrogels using 10 mM genipin at 60 °C have been reported to have a moduli between 60 and 100 kPa which is consistent with our results.³⁹ PBSA gels had a maximum strength near pH 3.5, which is consistent with reports of low pH albumin aggregation occurring

optimally in this pH range.⁴⁰ To the best of our knowledge, we are the first to report elastic modulus characterization of PBSA-type hydrogels. Their reduced stiffness suggests that PBSA hydrogels are not cross-linked, as in the case of TBSA hydrogels. Further decreasing the acidity of the protein solution below pH 3 resulted in nongelling viscous solutions. In 20 wt % hydrogels, cryo-SEM images show the presence of larger pore structures in the TBSA gels (Figure 1C) relative to those in the PBSA gels (Figure 1B). Rheological characterization demonstrated the rapid formation of TBSA hydrogels (17–65 s) in contrast to the slower kinetics in the PBSA hydrogels (330–2300 s). Furthermore, the evaluation of the hydrogel crossover points between the G' and G'' indicate a critical minimum protein concentration of 15 wt % for the formation of PBSA hydrogels.

The observed swelling of the PBSA gels in the β -ME solvent suggests that the 17 disulfide bonds remain intact during the fabrication of the gel. The observation that disruption of disulfide bridges by β -ME only tells us that the disulfide bridge network in the hydrogel is primarily intramolecular rather than intermolecular. Low pH alone is typically insufficient to break the intramolecular disulfide bonds in the absence of a strong reducing agents but it is possible that some intermolecular rearrangement has occurred. Regardless of the extent of intermolecular disulfide bonding, the disruption of the intramolecular disulfide bridges by β -ME in the hydrogel will certainly destabilize individual proteins and weaken the hydrogel overall even if intermolecular disulfide bonds are not present in large quantity. In the cryo-SEM images (Figure 1B), the structures appear very compact, with short persistence lengths. These results are consistent with higher critical protein concentrations needed for PBSA hydrogel formations. The observed swelling effect during β -ME exposure could be explained by a combination of increased hydrogel and protein flexibility due to reduced inter- and intramolecular disulfide bonds that enable the hydrogel to absorb more water.

Despite the identical composition of PBSA and TBSA hydrogels, differences in the *in vivo* degradation rate were observed and are likely attributable to differences in the mechanisms of hydrogel formation that led to the different gel microstructures (Figure 1B,C). The cryo-SEM images depicted a difference in the hydrogel porosity which has been noted by other groups to affect macrophage activity and capsule formation.^{41–43} It is also possible that the higher Young's modulus of the TBSA gels may have affected the cellular biodegradation process *in vivo*. It is well-known that matrix stiffness plays an important role as a mediator of cellular behavior. As a comparison, the well-studied Matrigel has an elastic modulus of 443 ± 285 Pa.⁴⁴ In 3D cell culture, cells tend to exert greater traction on stiffer hydrogel scaffolds than on weaker scaffolds⁴⁵ and tended to enhance cell spreading on 2D stiffness gradients.⁴⁶ In our results, PBSA hydrogels exhibited a matrix that was more conducive to cell infiltration than the TBSA hydrogels.

The primary objective of the simulation calculations was to determine whether F-form albumin has any binding affinity for atRA. The observation that 9 out of 10 atRA molecules became bound to the F-form albumin and the large calculated FSsite1 binding energy is encouraging as evidence that F-form albumin has significant residual binding affinity for atRA. There appears to be a critical balance between the forces that govern protein structural integrity with protein functionality, as reported by others.⁴⁷ While protein destabilization is required for hydrogel

formation, too much denaturation becomes a hindrance to protein functionality and biocompatibility. While this work only explores atRA binding, it is very likely that additional binding sites are available on domains II and III for numerous other therapeutic molecules that naturally have a binding affinity for N-form albumin. Reports in the literature have demonstrated the potent inhibitory effect of atRA on the migration of HASMC.^{48,49} The slow release of atRA from PBSA and TBSA hydrogels in significant quantities (50–200 ng) was demonstrated. The inhibitory effect of released atRA on HASMC migration was confirmed, indicating that the atRA remains bioactive after its release from the PBSA and TBSA hydrogels. The mechanism of formation for PBSA-hydrogels may also explain our preliminary observations, whereby gels were formed using fibrinogen or human blood plasma at low pH values. Therefore, electrostatically triggered partial denaturation may be used to engineer and study new natural hydrogel systems based solely on biomacromolecules.

CONCLUSIONS

We describe a new mechanism for the formation of partially denatured albumin hydrogels that retain intrinsic binding affinities associated with the normal configuration. In this procedure, lowering the solution pH enables albumin to transition into the F isoform driven by electrostatic interactions, which results in an exposure of core hydrophobic regions. Albumin in this conformation aggregates and forms bundled structures. At a critical concentration >15 wt %, the bundles form a percolating network that leads to the formation of a solid hydrogel with a Young's modulus ranging from 34 to 46 kPa depending on the protein concentration. The hydrogen ions required during PBSA hydrogel formation can be neutralized so that the resulting material has a physiological pH 7.4. PBSA hydrogels remain stable for up to three months and exhibit significant degradation and cellular infiltration after implantation *in vivo*, an improvement over TBSA hydrogels. We have shown that intrinsic drug binding properties of albumin to atRA are conserved in the N–F transformation using atomistic molecular dynamics simulations and *in vitro* by fluorescence quenching. Most importantly, atRA that is released from the PBSA hydrogels remains bioactive. This work emphasizes a true integration of multidisciplinary approaches that range from computational techniques to animal experiments and exemplifies a useful strategy for future biomaterials development.

ASSOCIATED CONTENT

S Supporting Information

Supporting videos. This material is available free of charge via the Internet at <http://pubs.acs.org>.

AUTHOR INFORMATION

Corresponding Author

*E-mail: g-ameer@northwestern.edu.

Notes

The authors declare no competing financial interest.

ACKNOWLEDGMENTS

This research was supported in part by the National Institutes of Health under Ruth L. Kirschstein National Research Service Award 1F31EB014698–01 from the National Institute of Biomedical Imaging and Bioengineering and by the Materials

Research Science and Engineering Center program of the NSF (DMR-0520513) at Northwestern University. We thank Yeshayahu (Ishi) Talmon and his research group at the Technion – Israel Institute of Technology for instrumentation and guidance in obtaining cryo-SEM images. We thank Kenneth Shull and Katie Otim at Northwestern for their help in providing instrumentation and guidance during mechanical indentation experiments. We thank Jisheng Xiao and Jian Yang for their assistance in collecting rheological data.

■ REFERENCES

- (1) Peters, T. *All About Albumin*; Elsevier: New York, 1995.
- (2) Peppas, N. A.; Hilt, J. Z.; Khademhosseini, A.; Langer, R. *Adv. Mater.* **2006**, *18* (11), 1345–1360.
- (3) Slaughter, B. V.; Khurshid, S. S.; Fisher, O. Z.; Khademhosseini, A.; Peppas, N. A. *Adv. Mater.* **2009**, *21* (32–33), 3307–3329.
- (4) Carter, D. C.; Ho, J. X. *Adv. Protein Chem.* **1994**, *45*, 153–203.
- (5) Baler, K.; Martin, O. A.; Carignano, M. A.; Ameer, G. A.; Vila, J. A.; Szleifer, I. *J. Phys. Chem. B* **2014**, *118* (4), 921–930.
- (6) Day, Y. S. N.; Myszka, D. G. *J. Biopharm. Sci.* **2003**, *92* (2), 333–343.
- (7) Barone, G.; Capasso, S.; DelVecchio, P.; DeSena, C.; Fessas, D.; Giancola, C.; Graziano, G.; Tramonti, P. *J. Therm. Anal.* **1995**, *45* (6), 1255–1264.
- (8) Chmelik, J.; Anzenbacher, P.; Chmelikova, J.; Matejckova, M.; Kalous, V. *Collect. Czech. Chem. Commun.* **1988**, *53* (2), 411–422.
- (9) Gianazza, E.; Galliano, M.; Miller, I. *Electrophoresis* **1997**, *18* (5), 695–700.
- (10) Clark, A. H.; Kavanagh, G. M.; Ross-Murphy, S. B. *Food Hydrocolloids* **2001**, *15* (4–6), 383–400.
- (11) Gosal, W. S.; Ross-Murphy, S. B. *Curr. Opin. Colloid Interface Sci.* **2000**, *5* (3–4), 188–194.
- (12) Haque, Z. Z.; Aryana, K. *J. Food Sci. Technol. Res.* **2002**, *8* (1), 1–3.
- (13) Matsudomi, N.; Rector, D.; Kinsella, J. E. *Food Chem.* **1991**, *40* (1), 55–69.
- (14) Navarra, G.; Giacomazza, D.; Leone, M.; Librizzi, F.; Militello, V.; Biagio, P. L. S. *Eur. Biophys. J.* **2009**, *38* (4), 437–446.
- (15) Renard, D.; Lefebvre, J. *Int. J. Biol. Macromol.* **1992**, *14* (5), 287–291.
- (16) Abraxis BioScience, LLC. Abraxane(R) for Injectable Suspension (paclitaxel protein-bound particles for injectable suspension). *Drugs.com*, 2005; Vol. *2010*, pp 1–20.
- (17) Christiansen, C.; Kryvi, H.; Sontum, P. C.; Skotland, T. *Biotechnol. Appl. Biochem.* **1994**, *19*, 307–320.
- (18) Iemma, F.; Spizzirri, U. G.; Puoci, F.; Muzzalupo, R.; Trombino, S.; Picci, N. *Drug Delivery* **2005**, *12* (4), 229–234.
- (19) Pande, S.; Vyas, S. P.; Dixit, V. K. *J. Microencapsulation* **1991**, *8* (1), 87–93.
- (20) Rubino, O. P.; Kowalsky, R.; Swarbrick, J. *Pharm. Res.* **1993**, *10* (7), 1059–1065.
- (21) Fanali, G.; di Masi, A.; Trezza, V.; Marino, M.; Fasano, M.; Ascenzi, P. *Mol. Aspects Med.* **2012**, *33* (3), 209–290.
- (22) Iemma, F.; Spizzirri, U.; Muzzalupo, R.; Puoci, F.; Trombino, S.; Picci, N. *Colloid Polym. Sci.* **2004**, *283* (3), 250–256.
- (23) Oss-Ronen, L.; Seliktar, D. *Adv. Biomater.* **2010**, *12* (1–2), 45–52.
- (24) Leggio, C.; Galantini, L.; Pavel, N. V. *Phys. Chem. Chem. Phys.* **2008**, *10* (45), 6741–6750.
- (25) Yamasaki, M.; Yano, H.; Aoki, K. *Int. J. Biol. Macromol.* **1990**, *12* (4), 263–268.
- (26) Vorobjev, Y. N.; Vila, J. A.; Scheraga, H. A. *J. Phys. Chem. B* **2008**, *112* (35), 11122–11136.
- (27) Hess, B.; Kutzner, C.; van der Spoel, D.; Lindahl, E. *J. Chem. Theory Comput.* **2008**, *4* (3), 435–447.
- (28) Van der Spoel, D.; Lindahl, E.; Hess, B.; Groenhof, G.; Mark, A. E.; Berendsen, H. J. C. *J. Comput. Chem.* **2005**, *26* (16), 1701–1718.
- (29) Lindahl, E.; Hess, B.; Van Der Spoel, D. *J. Mol. Model.* **2001**, *7* (8), 306–317.
- (30) Berendsen, H. J. C.; Vanderspoel, D.; Vandrunen, R. *Comput. Phys. Commun.* **1995**, *91* (1–3), 43–56.
- (31) Jorgensen, W. L.; Maxwell, D. S.; Tirado-Rives, J. *J. Am. Chem. Soc.* **1996**, *118* (45), 11225–11236.
- (32) Torrie, G. M.; Valleau, J. P. *Chem. Phys. Lett.* **1974**, *28* (4), 578–581.
- (33) Hub, J. S.; de Groot, B. L.; van der Spoel, D. *J. Chem. Theory Comput.* **2010**, *6* (12), 3713–3720.
- (34) Bellare, J. R.; Davis, H. T.; Scriven, L. E.; Talmon, Y. *J. Electron Microsc. Technol.* **1988**, *10* (1), 87–111.
- (35) Issman, L.; Talmon, Y. *J. Microsc.* **2012**, *246* (1), 60–69.
- (36) Lin, W. C.; Otim, K. J.; Lenhart, J. L.; Cole, P. J.; Shull, K. R. *J. Mater. Res.* **2009**, *24* (3), 957–965.
- (37) Maiti, T. K.; Ghosh, K. S.; Debnath, J.; Dasgupta, S. *Int. J. Biol. Macromol.* **2006**, *38* (3–5), 197–202.
- (38) Murata, M.; Tani, F.; Higasa, T.; Kitabatake, N.; Doi, E. *Biosci. Biotechnol. Biochem.* **1993**, *57* (1), 43–46.
- (39) Butler, M. F.; Clark, A. H.; Adams, S. *Biomacromolecules* **2006**, *7* (11), 2961–2970.
- (40) Bhattacharya, M.; Jain, N.; Mukhopadhyay, S. *J. Phys. Chem. B* **2011**, *115* (14), 4195–4205.
- (41) Annabi, N.; Nichol, J. W.; Zhong, X.; Ji, C. D.; Koshy, S.; Khademhosseini, A.; Dehghani, F. *Tissue Eng., Part B* **2010**, *16* (4), 371–383.
- (42) Linnes, M. P.; Ratner, B. D.; Giachelli, C. M. *Biomaterials* **2007**, *28* (35), 5298–5306.
- (43) Marshall, A. J.; Irvin, C. A.; Barker, T.; Sage, E. H.; Hauch, K. D.; Ratner, B. D. *Abst. Pap. ACS* **2004**, *228*, U386–U386.
- (44) Soofi, S. S.; Last, J. A.; Liliensiek, S. J.; Nealey, P. F.; Murphy, C. J. *J. Struct. Biol.* **2009**, *167* (3), 216–219.
- (45) Legant, W. R.; Miller, J. S.; Blakely, B. L.; Cohen, D. M.; Genin, G. M.; Chen, C. S. *Nat. Methods* **2010**, *7* (12), 969–U113.
- (46) Sunyer, R.; Jin, A. J.; Nossal, R.; Sackett, D. L. *PLoS One* **2012**, *7* (10), e46107.
- (47) El Kadi, N.; Taulier, N.; Le Huerou, J. Y.; Gindre, M.; Urbach, W.; Nwigwe, I.; Kahn, P. C.; Waks, M. *Biophys. J.* **2007**, *402A*–402A.
- (48) Axel, D. I.; Frigge, A.; Dittmann, J.; Runge, H.; Spyridopoulos, I.; Riessen, R.; Viebahn, R.; Karsch, K. R. *Cardiovasc. Res.* **2001**, *49* (4), 851–862.
- (49) Neuville, P.; Yan, Z. Q.; Gidlof, A.; Pepper, M. S.; Hansson, G. K.; Gabbiani, G.; Sirsjo, A. *Arterioscler., Thromb., Vasc. Biol.* **1999**, *19* (6), 1430–1436.